Dual-loop control strategy applied to the cluster of multiple nanogrids for rural electrification applications

Nasir, Mashood; Anees , Muhammad; Khan, Hassan Abbas; Guerrero, Josep M.

Published in:
IET Smart Grid

DOI (link to publication from Publisher):
10.1049/iet-stg.2019.0098

Publication date:
2019

Document Version
Publisher's PDF, also known as Version of record

IET Smart Grid

Special Section: Selected Papers from the 7th IET Renewable Power Generation Conference (RPG 2018)

IET Journals
The Institution of Engineering and Technology

Dual-loop control strategy applied to the cluster of multiple nanogrids for rural electrification applications

eISSN 2515-2947
Received on 29th March 2019
Revised 12th June 2019
Accepted on 24th June 2019
E-First on 24th July 2019
doi: 10.1049/iet-stg.2019.0098
www.ietdl.org

Mashood Nasir[1,2] ✉, Muhammad Anees[1], Hassan Abbas Khan[1], Josep M. Guerrero[2]

[1]*Department of Electrical Engineering, Lahore University of Management Sciences, Lahore, Pakistan*
[2]*Department of Energy Technology, Aalborg University, Aalborg, Denmark*
✉ *E-mail: mashood.nasir@lums.edu.pk*

Abstract: In this study, a dual-loop control strategy is applied to a highly distributed architecture of photovoltaic/battery-based DC microgrid built through an interconnection of a cluster of multiple nanogrids. Typically, in these distributed architectures, resource sharing among the spatially distributed nanogrids is enabled via communication-based control methodologies, which adds cost and complexity to the overall system. Alternately, a communication-less and decentralised control methodology is proposed which utilises inner loop current control and outer loop voltage droop (*V–I* droop) control for the coordinated resource sharing among the distributed resources. The proposed control scheme adapts various modes based on the local measurements of bus voltage and battery state of charge, therefore, offers a distributed solution, omitting the need for centralised communication control. Various scenarios of power sharing among the contributing nanogrids are evaluated through the proposed multi-mode adaptive control. The efficacy of the proposed control scheme is validated through simulations on MATLAB/Simulink and laboratory scale hardware prototype. Results show that the proposed decentralised control strategy is capable to ensure stable and coordinated operation without any dedicated layer of communication among the dispersed generation/storage resources.

Nomenclature

Nomenclature used throughout this paper is stated below for quick reference. Other symbols are defined as needed.

A. Indexes

T	instant of time ranging from 1 to T
I	SHS number ranging from 1 to N

B. Parameters

N	number of houses in the village
P_i^{PV}	PV power generated by the ith house (W)
I_i^{PV}	PV current generated by the ith house (A)
P_i^{L}	load power demand of the ith house (W)
I_i^{load}	load current demand of the ith house (A)
V_{ref}	reference voltage of the DC bus (V)
V^{B}	output voltage of the DC bus (V)
V^{L}	lower threshold of DC bus voltage (V)
V^{H}	upper threshold of DC bus voltage (V)
SOC_i	state of charge of battery at the ith house (%)
SOC^0	initial state of charge of the battery (%)
$\mathrm{SOC}_i^{\min}$	lower threshold of battery SOC (%)
$\mathrm{SOC}_i^{\max}$	upper threshold of battery SOC (%)
R_{d}	constant droop impedance (Ω)
R_{dis}	discharging droop impedance (Ω)
R_{ch}	charging droop impedance (Ω)
I_{ref}^i	reference current for the ith interfacing converter (A)
$K_{\mathrm{p,v}}$	proportional coefficient for outer voltage loop
$K_{\mathrm{p,i}}$	proportional coefficient for inner current loop
$K_{\mathrm{i,v}}$	integral coefficient for outer voltage loop
$K_{\mathrm{i,i}}$	integral coefficient for inner current loop

1 Introduction

Access to electricity plays an important role in enhancing the socio-economic growth of a community [1]. Reliable access to electricity is extremely crucial for human well-being and can contribute to better health, employment, agriculture, and education opportunities. On the contrary, unavailability of electricity hampers the basic human rights including access to clean drinking water, proper lighting, and sustainable employment opportunities; therefore, declines the socio-economic status and tends to enhance the poverty [2]. According to the international energy agency, over 1,000,000,000 people, i.e. 14% of the global population do not have access to electricity [3]. The inhabitants of these regions rely on unhealthy resources such as kerosene oil for lighting and other applications causing many adverse effects on individuals as well as environment [4, 5]. Therefore, a higher focus on clean electrification is seen in recent years to help many developing regions attain access to electricity and subsequent sustainable development.

Solar photovoltaic (PV) and battery-based islanded DC microgrids are becoming very popular for the off-grid electrification due to decreasing PV costs as well as higher efficiency distributed generation [6–8]. Currently, commercial deployments either use (a) centralised architecture with PV generation and battery storage at a centralised location or (b) distributed architecture with either generation or storage or both are spatially distributed [9]. Centralised architectures have an advantage from installation, control, operation, and maintenance perspective. However, these have high distribution losses for higher-power delivery [10, 11]. Moreover, these architectures need centralised planning at the very outset requiring large upfront system costs [12]. Prominent centralised installations include plants in Chhattisgarh, Sunderbans, and Lakshadweep in India [13, 14]. Similarly, Mera Gao Power in Utter Pradesh, India and the Jabula project in Cape Town, South Africa are other successful models of electrification via PV/battery-based islanded DC microgrids [15].

Distributed architectures can have partially or highly distributed architectures, where generation, as well as storage, can be distributed spatially. These systems have lower distribution losses and are generally scalable compared with rigidly centralised

architectures [16–18]. Their modular nature imparts scalability to the overall microgrid structure; thereby, centralised planning and upfront installation of resources not mandatory for these distributed architectures. Rather, in such topologies, multiple household-level energy systems are interconnected to formulate a microgrid, where each household may operate independently as well as in coordination. Furthermore, these systems can have provisions of sharing power at the neighbourhood level with the capability to extract the benefit of usage diversity at a village scale [19]. A comprehensive review of the existing control strategies and stabilisation techniques is presented in [20]. It has been shown that DC microgrid control can be categorised as decentralised, centralised, or distributed control systems. Decentralised control strategies are generally based on localised measurement; therefore, do not employ require communication. While centralised and distributed control scheme requires communication at the cost of enhanced functionalities including economic dispatch and transactive energy applications along with better stability margins. Similarly, Amini *et al.* [21] presented a cloud-based optimal power routeing control algorithm for the cluster of DC microgrids using communication environment emulated by OMNeT++. Other than that there exist many distributed control algorithms in the literature focusing on optimal power flow among the cluster of multiple micro/nanogrids, e.g. distributed tertiary control presented in [22], distributed economic model predictive control presented in [23], and multi-agent system-based distributed control presented in [24]. However, all the distributed control schemes require sophisticated communication among the distributed resources for their stable and coordinated operation. The involvement of dedicated communication resources will not only add to the cost of the system but will also enhance the complexity of the operation. From the perspective of rural electrification, such a complex and cost prohibitive solution is generally considered unviable for wide-scale adoption.

Alternately, various communication-less decentralised control schemes have been presented in the literature. For instance, Nasir *et al.* [17] presented a hysteresis-based voltage droop algorithm that adjusts the duty cycle of interfacing converters for stable operation of the distributed microgrid. However, it does not consider the coordinated resource sharing and every contributing node supplies or receives a constant amount of power irrespective of its own resource availability. So our first contribution lies in proposing a decentralised and communication-less control schematic capable of coordinated resource sharing based on the resource availability in an individual household suitable for developing villages with limited economic resource availability. A dual-loop adaptive droop control scheme presented by Lu *et al.*[25] consider the partial coordination of distributed resources proportional to the battery state of charge (SOC) index during power supply mode (battery discharge mode). However, it does not consider power sharing in proportional to the SOC index during the charging mode of the battery. This results in suboptimal operation, where all discharged batteries will get charged at the same rate irrespective of their resource deficiency. Also, the proposed scheme causes excessive distribution losses for unwanted SOC balancing and undesired charging/discharging of batteries in various households.

Subsequently, Nasir *et al.* [26] presented a fully coordinated adaptive droop scheme that considers resource sharing in proportional to the SOC index for both charging and discharging. This scheme has an advantage as it employs an adaptive *I–V* droop method which has superior transient performance in comparison with the *V–I* droop. However, the stability margins for *I–V* droop control are relatively smaller in comparison with *V–I* droop control; therefore, it may be subjected to instability due to the involvement of multiple constant power loads in the microgrid structure [27, 28]. So, our second contribution lies in proposing a relatively more stable and robust control scheme with enhanced stability margins, capable to deal with versatile conditions of power sharing among the nanogrid cluster.

To rectify these stability limitations, and enable communication-less resource sharing in a coordinated manner, an adaptive dual-loop control strategy has been presented in [29]. This decentralised scheme employs *V–I* droop control for enhanced stability margins through configuring *V–I* droop, as a function of SOC index of the contributing battery. This results in each node contributing to power sharing, in accordance with its resource availability. However, Nasir *et al.* [29] discuss only the dual-loop control of the bidirectional converter (responsible for power sharing among multiple nanogrids) without highlighting the control schematics for the solar converter (responsible for optimal power extraction from PV panel). Therefore, it does not consider the operation of the microgrid in extreme condition, i.e. when excessive solar resources are available, while nanogrid load demand is minimal and microgrid voltage is at its saturation limit. If solar PV generation through solar converter is not controlled in such extreme conditions, it may result in the system overvoltages and may also instigate instability in the microgrid system. Moreover, Nasir *et al.* [29] present only simulation results, without their validation on a hardware platform. So, our third contribution lies in extending the control modes through the local coordination of solar converter (responsible for optimal power extraction from the solar panel) with the bidirectional converter (responsible for power sharing among neighbouring nanogrids) to handle the extreme conditions of operation. This extended coordination among the nanogrid converters and controlled power generation from solar PV results in enhanced stability of the system as demonstrated through simulation results. Moreover, a hardware prototype is developed and simulation results for the extended control are validated through laboratory scale hardware prototype.

This paper is organised as follows: Section 1 explains the need for rural electrification through a bottom-up approach using clusters of multiple nanogrids and individual solar home systems. It also discusses the relevant existing literature and key contributions to the scope of the presented work. Section 2 highlights the structure of the highly distributed PV/battery-based DC microgrid and its individual components. A nanogrid is considered as a building block and subsequent integration of these nanogrids through the proposed decentralised control yields the overall microgrid operation. Section 3 presents the power electronic interface in each nanogrid along with the multi-mode adaptive algorithm for the decentralised control. Since the overall control is based on the local measurements only and there is no communication link for the information sharing among multiple nanogrids; therefore, decentralised control schematics for both of the converters in an individual nanogrid are highlighted in Section 3. To evaluate the efficacy of the decentralised control scheme, a case study is presented in Section 4. Therefore, Section 4 presents the simulation and hardware results for various possible power-sharing scenarios. Also, a comparative study of other possible droop realisation for the decentralised control is presented in Section 4. On the basis of the results, conclusions are drawn in Section 5.

2 Microgrid architecture as an interconnection of nanogrids cluster

Fig. 1 shows a highly distributed architecture of solar PV DC microgrid built through an interconnection of a cluster of N nanogrids [17]. An individual household in a village having its own PV generation, battery storage, solar converter, and DC loads can be termed as a nanogrid. These nanogrids can be integrated through a bidirectional converter and DC bus to formulate a village scale microgrid, where multiple nanogrids can exchange resources based on their local requirements. Each household/nanogrid has two converters, where *Conv* a_i is the solar converter responsible for optimal power extraction from PV and *Conv* b_i is the interface converter responsible for the bidirectional exchange of power between multiple households through DC bus. The battery acts as a buffer and provides a balance between PV power generation P^{PV}, local load consumption P^{L}, and power transferred to or from the interconnecting DC bus P^{G}. Therefore, battery acts as a point of common coupling at which the terminals of both converters and load terminals are connected. Since battery and load voltage levels are same, therefore, an extra converter in the path from the battery

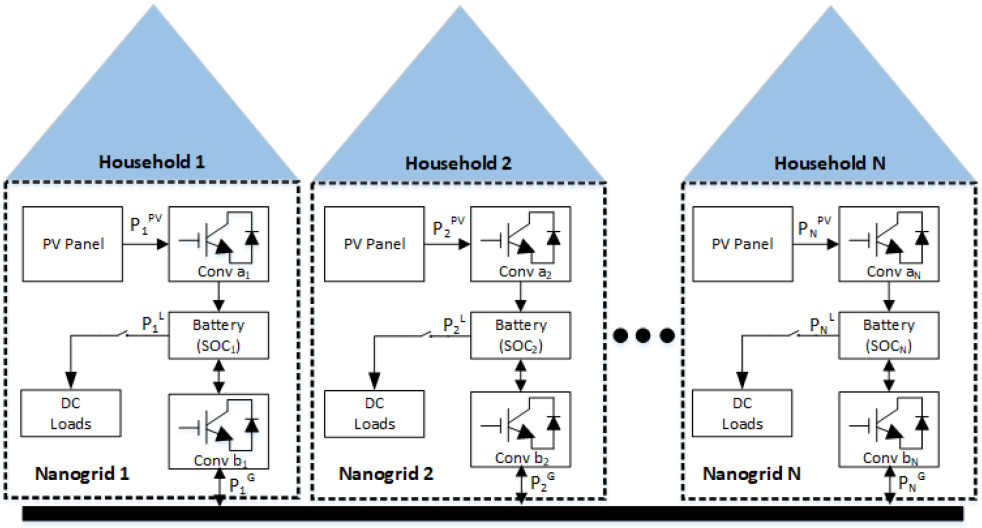

Fig. 1 *DC microgrid architecture built through the interconnection of a cluster of multiple nanogrids*

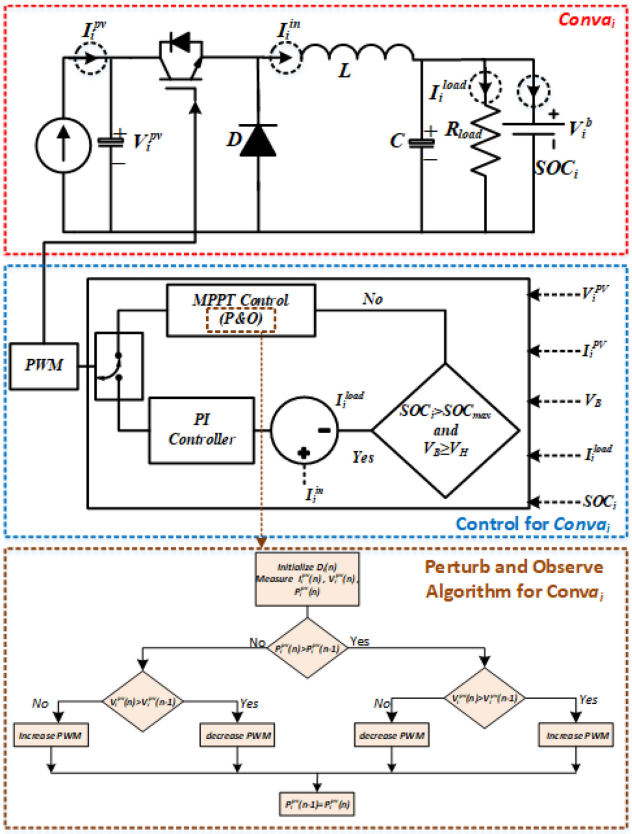

Fig. 2 *Power electronic circuit and multi-mode control scheme for solar converter*

to the load is not needed, rather a switch (fuse/relay is used to control the maximum allowable power to be transferred to the local load). The overall energy balance at the ith nanogrid can be represented in terms of battery SOC SOC_i through energy balance equation

$$\mathrm{SOC}_i(t) = \mathrm{SOC}_i^0 + \frac{1}{C_i}\int_0^T \left(P_i^{\mathrm{PV}} - P_i^{\mathrm{L}} - P_i^{\mathrm{G}}\right)\mathrm{d}t \qquad (1)$$

where C_i is the energy capacity (Wh) of the battery installed in the ith nanogrid and $\mathrm{SOC}_i^{\mathrm{o}}$ is its initial SOC. SOC acts as a key indicator for energy resource availability in an individual nanogrid and multi-mode adaptive algorithm is, therefore, based on this parameter. Another important parameter indicating the energy resource availability in overall microgrid network is DC bus voltage V^{B}, and therefore the multi-mode adaptive algorithm also takes into account while deciding the mode of operation and associated power sharing. Since both of these parameters are available locally at each nanogrid, therefore, a control algorithm based on these two parameters will omit the need of centralised communication controller and the desired coordination will be achieved through decentralised control. The coordinated resource sharing feature is enabled via the proposed adaptive dual-loop control (inner current and outer voltage loop) of the bidirectional converter *Conv* b_i and is detailed in the next section. To tackle the excessive power generation conditions when PV generation is more than the battery capacity or local load requirements, the control of solar converter *Conv* a_i also adapts multiple modes based on these two parameters. The extended control modes for *Conv* a_i are also discussed in the next section.

3 Decentralised control algorithm

On the basis of the local measurements of SOC_i and DC bus voltage V^{B} at the ith nanogrid, solar converter *Conv* a_i, and the bidirectional interface converter *Conv* b_i can adapt the following modes.

3.1 Control scheme for solar converter Conv a_i

The power electronic circuit, control diagram, and multiple modes adapted by solar converter *Conv* a_i during different modes of operations are shown in Fig. 2. These modes are dictated by battery SOC and DC bus voltage V^{B}. On the basis of the battery capacity, maximum and minimum thresholds on battery SOC, i.e. $\mathrm{SOC}_{\max}$ and $\mathrm{SOC}_{\min}$ are defined. A value of SOC below $\mathrm{SOC}_{\min}$ indicates that nanogrid energy availability is low and battery needs to be charged, while a value of SOC above $\mathrm{SOC}_{\max}$ indicates that excessive energy for neighbourhood-level exchange is available.

The algorithm processes PV panel voltage V_i^{PV} and current I_i^{PV} for optimal power extraction from the PV panel at a given solar irradiance. During normal operating conditions when household requirements are higher than solar PV generation or battery is not fully charged, i.e. $\mathrm{SOC}_i < \mathrm{SOC}_{\max}$, solar converter operates in maximum power point tracking (MPPT) mode. Various MPPT algorithms for optimal solar power extraction under uniform and non-uniform irradiance conditions are discussed in the literatures [30, 31]; however, in this work, perturb and observe is used due to its inherent simplicity and ease of applicability [30].

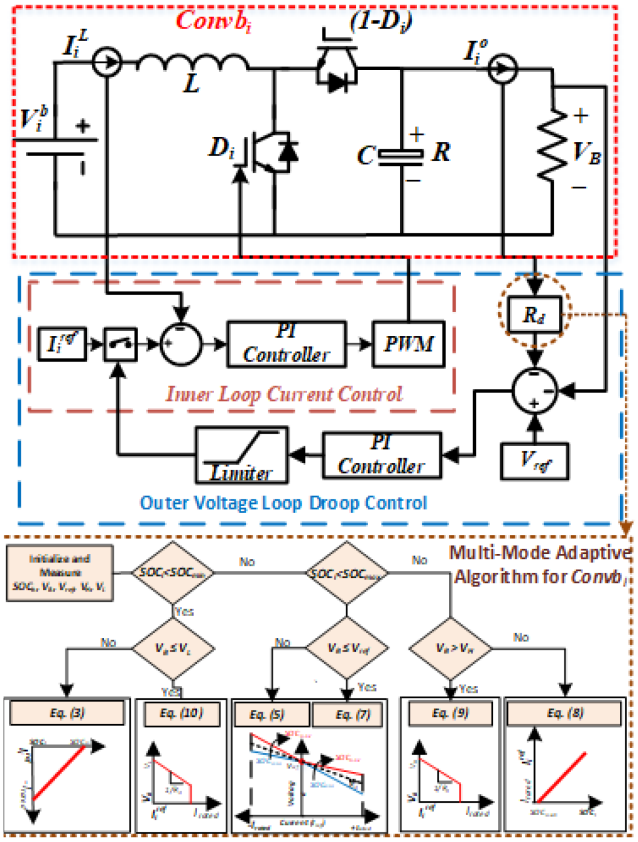

Fig. 3 *Power electronic circuit and multi-mode control scheme for bidirectional interface converter*

3.2 Control scheme for bidirectional interface converter Conv b_i

The power electronic converter circuit, control diagram, and multiple modes adapted by solar converter *Conv* a_i during different modes of operations are shown in Fig. 3. To interconnect multiple households without any physical communication layer among the dispersed resources, an adaptive control scheme is used for each bidirectional converter *Conv* b_i. On the basis of localised measurements of bus voltage V^{B} and battery SOC converter may shift its mode of operation between (a) current controlled charging mode (CCCM), (b) current controlled discharging mode (CCDM), (c) dual-loop adaptive *V–I* droop mode, and (d) constant *I–V* droop mode. In each of these four modes, a current reference I_{ref} is generated as governed by (3)–(10). The inner loop proportional–integral (PI) current controller then generates the duty cycle D such that the desired current reference is achieved and the battery is charged or discharged at the desired value of current

$$D = K_{\mathrm{p,\,i}}(I_{\mathrm{ref}} - I_{\mathrm{in}}) + K_{\mathrm{i,\,i}}\int_0^t (I_{\mathrm{ref}} - I_{\mathrm{in}})\mathrm{d}t \tag{2}$$

where $K_{\mathrm{p,i}}$ and $K_{\mathrm{i,i}}$ are the PI constants for inner current loop PI controller and I_{in} is the inductor current of the bidirectional converter at which battery is charged or discharged. Thus, by controlling the current sharing of each individual household based on the adaptive control strategy, a decentralised control ensuring stable and coordinated operation of the microgrid is achieved.

3.2.1 Current controlled charging mode: SOC index of the battery serves as an indicator of the resource availability in an individual nanogrid. Similarly, DC bus voltage V^{B} serves as an indicator of the resource availability in the overall microgrid structure. When SOC falls below the minimum threshold, i.e. $\mathrm{SOC}<\mathrm{SOC}_{\mathrm{min}}$ but $V^{\mathrm{B}}>V^{\mathrm{L}}$, i.e. DC bus voltage is higher than the minimum allowable V^{L} interface converter switches in CCCM. The current reference is generated based on the extent of resource deficiency such that it demands rated current I_{rated} when it is away from $\mathrm{SOC}_{\mathrm{min}}$ and its current demand decreases as its SOC reaches to $\mathrm{SOC}_{\mathrm{min}}$. The PI controller then generates the duty cycle such that the desired current reference is achieved and the battery is charged at the desired value of current governed by the equation below:

$$I_{\mathrm{ref}} = I_{\mathrm{rated}}\left(\frac{\mathrm{SOC}}{\mathrm{SOC}_{\mathrm{min}}} - 1\right) \tag{3}$$

3.2.2 Dual-loop adaptive voltage droop control (V–I) mode: In the intermediate range of SOC, i.e. $\mathrm{SOC}_{\mathrm{min}}\leq\mathrm{SOC}\leq\mathrm{SOC}_{\mathrm{max}}$, each household has sufficient resource availability; therefore, it can either supply or demand power based on the requirements of neighbouring households. DC bus voltage V^{B} again serves as an indicator of the requirements of neighbouring households. A value of V^{B} below the reference voltage V_{ref} indicates that one or more neighbouring houses in the microgrid are deficient in resources and they need to be charged. At this point, the households having higher resource availability, i.e. having higher SOC index should supply more power in comparison with those households which have relatively lower resource availability. This coordination is ensured through a modified discharging droop R_{dis} given by (4), whose visual depiction is also shown in Fig. 3

$$R_{\mathrm{dis}} = R_{\mathrm{d}}\left[1 - 0.5\left(\frac{\mathrm{SOC} - \mathrm{SOC}_{\mathrm{min}}}{\mathrm{SOC}_{\mathrm{max}} - \mathrm{SOC}_{\mathrm{min}}}\right)\right] \tag{4}$$

R_{dis} ensures that virtual droop impedance R_{d} which is generally considered constant in a conventional *V–I* droop is decreasing here in a linear fashion from R_{d} to $0.5R_{\mathrm{d}}$ when SOC varies from $\mathrm{SOC}_{\mathrm{min}}$ to $\mathrm{SOC}_{\mathrm{max}}$. On the basis of this varying droop function R_{dis}, an outer voltage droop loop generates a reference for an inner loop current control as shown in Fig. 3 and given by the equation below:

$$I_{\mathrm{ref}} = K_{\mathrm{p,\,v}}\left(V_{\mathrm{ref}} - V^{\mathrm{B}} - I_{\mathrm{o}}R_{\mathrm{dis}}\right) + K_{\mathrm{i,\,v}}\left(V_{\mathrm{ref}} - V^{\mathrm{B}} - I_{\mathrm{o}}R_{\mathrm{dis}}\right) \tag{5}$$

where $K_{\mathrm{p,v}}$ and $K_{\mathrm{i,v}}$ are the PI constants for outer voltage loop PI controller and I_{o} is the output current of the bidirectional converter toward DC bus. Similarly, V^{B} above the reference voltage V_{ref} indicates that one or more neighbouring houses are already saturated and they need to be discharged. Therefore, in this situation, the households having lower resource availability, i.e. having lower SOC index should receive more power in comparison with those households which have relatively higher resource availability. This coordination is ensured through a modified charging droop R_{ch} given by (6), whose visual depiction is also shown in Fig. 3. R_{dis} ensures that virtual droop impedance R_{d} which is generally considered constant in a conventional *V–I* droop is increasing here in a linear fashion from $0.5R_{\mathrm{d}}$ to R_{d} when SOC varies from $\mathrm{SOC}_{\mathrm{min}}$ to $\mathrm{SOC}_{\mathrm{max}}$

$$R_{\mathrm{ch}} = 0.5R_{\mathrm{d}}\left[1 + \left(\frac{\mathrm{SOC} - \mathrm{SOC}_{\mathrm{min}}}{\mathrm{SOC}_{\mathrm{max}} - \mathrm{SOC}_{\mathrm{min}}}\right)\right] \tag{6}$$

On the basis of this varying droop function R_{ch}, an outer voltage droop loop generates a reference for an inner loop current control as shown in Fig. 2 and given by (6)

$$I_{\mathrm{ref}} = K_{\mathrm{p,\,v}}\left(V_{\mathrm{ref}} - V^{\mathrm{B}} - I_{\mathrm{o}}R_{\mathrm{ch}}\right) + K_{\mathrm{i,\,v}}\left(V_{\mathrm{ref}} - V^{\mathrm{B}} - I_{\mathrm{o}}R_{\mathrm{ch}}\right) \tag{7}$$

where $K_{\mathrm{p,v}}$ and $K_{\mathrm{i,v}}$ are the PI constants for outer voltage loop PI controller and I_{o} is the input current of the bidirectional converter from DC bus. Fig. 3 shows the variations of *V–I* droop as a function of SOC. It can be seen that for positive values of current I_{ref}, i.e. when an individual household is supplying power, moving from $\mathrm{SOC}_{\mathrm{min}}$ to $\mathrm{SOC}_{\mathrm{max}}$ decreases the slope of *V–I* curve, and therefore a household with a higher value of SOC supplies more

Table 1 Parameters of simulated case study

Description of the parameter	Value
number of nanogrids/households	4
input capacitance of each *Conv* b_i	220 μF
inductance of each *Conv* b_i	2.1 mH
inductance of each *Conv* a_i	500 μH
DC bus capacitance	10 mF
switching frequency for *Conv* a_i and *Conv* b_i	10 kHz
battery capacity for each household	2400 Wh
rated charging current for the battery	10 A
rated voltage of each battery	24 V
maximum threshold of battery SOC	80%
minimum threshold of battery SOC	30%
reference voltage for DC bus	48 V
initial voltage of DC bus	24 V
droop coefficient for each *Conv* a_i	0.21 Ω
droop coefficient for each *Conv* b_i	0.23 Ω
parameters of current loop controller	0.33, 15
parameters of voltage loop controller	1.75, 10

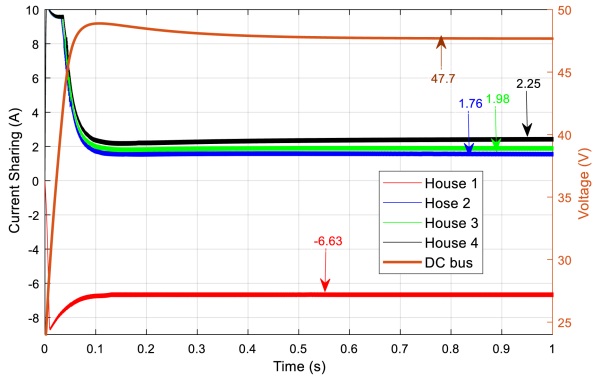

Fig. 4 *Simulation results for current sharing and DC bus voltage in case 1*

power in comparison with household having a lower value of SOC. Similarly, for negative values of current I_{ref}, i.e. when an individual household is receiving power, moving from SOC_{min} to SOC_{max} increases the slope of V–I curve, and therefore a household with a lower value of SOC receives more power in comparison with household having a higher value of SOC and vice versa.

3.2.3 Current controlled discharging mode: When SOC of the battery in an individual household increases above maximum threshold due to higher incident solar irradiance and associated PV power generation, i.e. $SOC>SOC_{max}$, and the neighbouring nanogrids have the capacity to absorb the excessive power, i.e. $V^B<V^H$, its bidirectional converter switches in CCDM. The current reference is generated based on the extent of resource saturation such that it supplies rated current I_{rated} when it is away from SOC_{max} and its current supply decreases as its SOC reaches to SOC_{max}. The PI controller then generates the duty cycle such that the desired current reference is achieved and the battery is discharged at the desired value of current governed by the equation below:

$$I_{ref} = I_{rated}\left(\frac{SOC_i - SOC_{max}}{100 - SOC_{max}}\right) \quad (8)$$

3.2.4 Constant I–V droop mode: Extreme operation conditions occur when solar PV generation is much higher than local as well as global load requirements, i.e. when $SOC>SOC_{max}$ and $V^B>V^H$ or when PV generation and battery storage energy is lower than load requirements, i.e. when $SOC<SOC_{max}$ and $V^B<V^L$. In these extreme conditions, bidirectional interface converter switches in constant I–V droop mode, thereby fixing the DC bus voltage at allowable limits, i.e. V^H or V^L. The current reference in these extreme conditions is given by (9) and (10). It is important to reiterate that in excessive generation condition solar converter changes its mode of operation from MPPT to current control mode

$$I^{ref} = \frac{1}{R_d}(V_H - V_B); \quad \text{if } V_B \geq V_H \quad (9)$$

$$I^{ref} = \frac{1}{R_d}(V_L - V_B); \quad \text{if } V_B \leq V_L \quad (10)$$

4 Results and discussion

For the validation of the proposed control scheme and associated power coordination, various test cases are analysed via simulations and laboratory scale hardware prototype.

4.1 Simulation results

For the validation of the proposed control scheme, simulations are carried out in MATLAB/Simulink using physical models of the converters and control schematic shown in Figs. 2 and 3. Various parameters for simulation are also shown in Table 1. The droop value R_d is selected according to the converter ratings and adjusted such that voltage of the microgrid is stable for its full range of operation. Similarly, integral and proportional parameters for current loop and voltage loop controllers are chosen based on the closed-loop stability of the proposed scheme.

4.1.1 One house is in CCCM and remaining houses are in V–I droop mode: In this scenario, battery of house 1 is assumed below minimum threshold of SOC, *i.e.* $SOC_1 = 10\%$, while the batteries of the other three households are assumed within the specified maximum and minimum thresholds, i.e. $SOC_2 = 35\%$, $SOC_3 = 55\%$, and $SOC_4 = 75\%$. The results of current sharing through the proposed decentralised control scheme are shown in Fig. 4. From Fig. 4, it can be seen that house 1 is demanding power in proportion to its resource deficiency as governed by (3), whereas houses 2–4 are supplying power in proportion to their resource availability such that house 4 having highest resource availability (SOC index) is supplying highest amount of current and house 2 is supplying lowest value of current for charging the battery of house 1.

4.1.2 One house is in CCDM and remaining houses are in V–I droop mode: In this scenario, battery of house 1 is assumed above maximum threshold of SOC, *i.e.* $SOC_1 = 90\%$, whereas the batteries of the other three households are assumed within the specified maximum and minimum thresholds of SOC, i.e. $SOC_2 = 35\%$, $SOC_3 = 55\%$, and $SOC_4 = 75\%$. The results of current sharing through the proposed decentralised control scheme are shown in Fig. 5. From Fig. 5, it can be seen that house 1 is supplying power in proportion to its resource saturation as governed by (8), whereas houses 2–4 are absorbing power in proportion to their resource deficiency such that house 2 having lowest resource availability (SOC index) is receiving highest amount of current and house 4 is receiving lowest value of current for charging their batteries from house 1.

4.1.3 One house is in CCCM, one house in CCDM, and remaining houses are in V–I droop mode: In this scenario, battery of house 1 is assumed below minimum threshold of SOC, *i.e.* $SOC_1 = 15\%$, battery of house 2 is assumed above minimum threshold of SOC, *i.e.* $SOC_2 = 95\%$, whereas the batteries of the other two households are assumed within the specified maximum and minimum thresholds of SOC, i.e. $SOC_3 = 55\%$ and $SOC_4 = 75\%$. The results of current sharing through the proposed decentralised control scheme are shown in Fig. 6. From Fig. 6, it can be seen that house 1 is demanding power in proportion to its

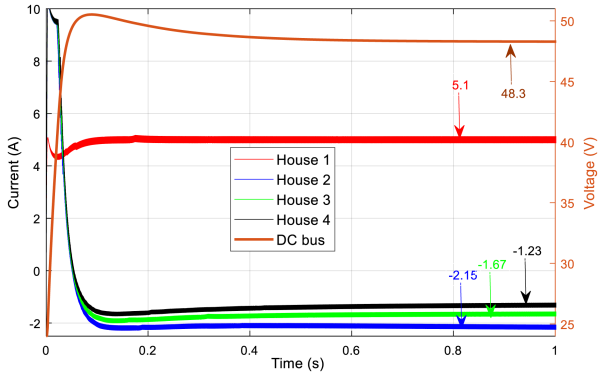

Fig. 5 *Simulation results for current sharing and DC bus voltage in case 2*

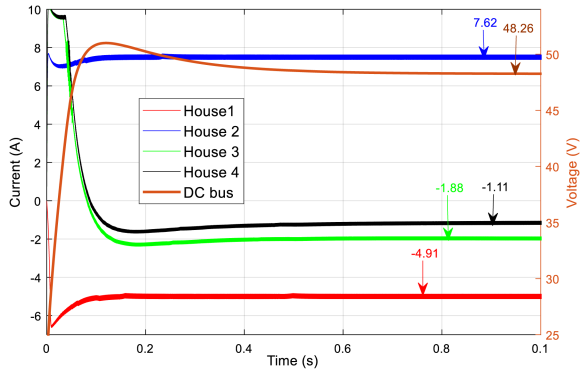

Fig. 6 *Simulation results for current sharing and DC bus voltage in case 3*

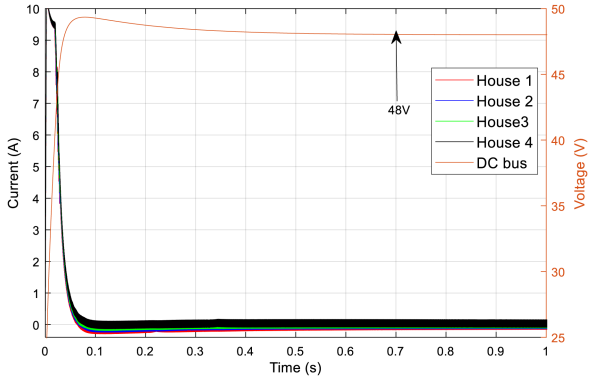

Fig. 7 *Simulation results for current sharing and DC bus voltage in case 4*

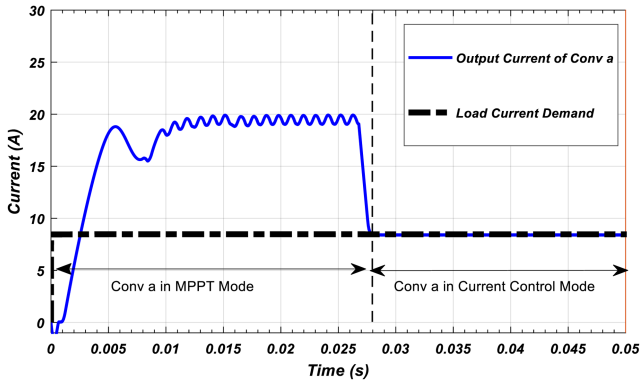

Fig. 8 *Simulation results for the transition between MPPT and CCM in excessive generation condition*

resource deficiency as governed by (3) and house 2 is supplying power in proportion to its resource saturation as governed by (8).

In this scenario, houses 3 and 4 will supply/demand power in accordance with the net current supplied at DC bus and its resulting voltage. Since in this scenario, net current supplied by house 2 is higher than the current absorbed by house 1; therefore, net voltage of DC bus is higher than V_{ref}, as a result of which houses 3 and 4 are absorbing power in accordance with their resource deficiency such that household 2 being at lower SOC is being charged at relatively higher current in comparison with household 3 as shown by Fig. 6.

4.1.4 All four houses are in V–I droop mode: In this scenario, all four houses are assumed within the maximum and minimum threshold range of SOC. Results of current sharing and DC bus voltage are shown in Fig. 7. Since all the houses are self-sufficient and are operating in *V–I* droop mode; therefore, voltage is stable at V_{ref} and there is no net power flow from one household to other via DC bus. In an optimally sized DC microgrid [32], households will be operating in this mode for most of the times; therefore, distribution losses will be minimum from generation end to utilisation end. This reduction in losses is otherwise not possible with the SOC balancing-based methodology presented in [25].

4.1.5 All four houses are in constant I–V droop mode and excessive generation is available: In this scenario, all four houses are assumed at the maximum SOC, i.e. $\text{SOC}_1 = \text{SOC}_2 = \text{SOC}_3 = \text{SOC}_4 = 85\%$. As a result of which all households will try to supply power to the neighbouring houses in accordance with (8). Consequently, grid voltage V^{B} will start increasing. When V^{B} will attain its maximum allowable voltage, i.e. V^{H}, *Conv* a_i will shift its mode of operation from MPPT mode to current controlled mode (CCM).

While *Conv* b_i for each house will shift its mode to constant *I–V* droop mode given by (9). In this mode of operation, *Conv* a_i will curtail the PV power generation in accordance with the household load current demand. This transition between MPPT and CCM is shown in Fig. 8. For instance, in Fig. 8, a constant load current demand 0f 9 A is considered. In the start of the simulation, when the converter is operating in MPPT mode, the current generated by PV is at MPP, i.e. 20 A. At $t = 0.028$ s, converter shifts its mode of operation and curtails current demand equal to household current demand, i.e. 9 A. Therefore, this extended control allows the transition from MPPT mode to CCM and avoids overvoltage instability in excessive generation conditions.

4.1.6 Comparative results of V–I droop control with I–V droop control: The results of the *V–I* droop control used in this scheme are compared with the *I–V* droop control strategy presented in [26, 33]. Fig. 9 shows the comparison of the proposed controller's performance (*V–I* droop) in comparison with the controller presented in [26, 33] (*I–V* droop). For the comparative analysis case, the battery of house 1 is assumed below the minimum threshold of SOC, i.e. $\text{SOC}_1 = 10\%$, whereas the batteries of the other three households are assumed within the specified maximum and minimum thresholds, i.e. $\text{SOC}_2 = 35\%$, $\text{SOC}_3 = 55\%$, and $\text{SOC}_4 = 75\%$. From Fig. 9, it can be observed that the steady-state response of both of the controllers converges to the same point; therefore, associated current sharing and DC bus voltages are same in the steady state as presented in case 1.

For the purpose of clarity, only the results of current sharing from house 1 and house 4, along with the DC bus voltage variations are highlighted in Fig. 9. Furthermore, it may be noted that *I–V* control exhibits relatively faster dynamics with a lower settling time as compared with *V–I* droop; however, due to the involvement of two loops, *V–I* droop exhibits superior stability characteristics and perform its intended operation over a wide range of droop coefficients [28].

4.2 Hardware results

For the validation of the proposed control scheme, a laboratory scale hardware prototype is developed as shown in Fig. 10. The converters for three nanogrids are designed and the integration of three nanogrids is achieved through DC bus interconnection emulated via a large capacitor and battery as shown in Fig. 10. Various other hardware parameters are detailed in Table 2. Various

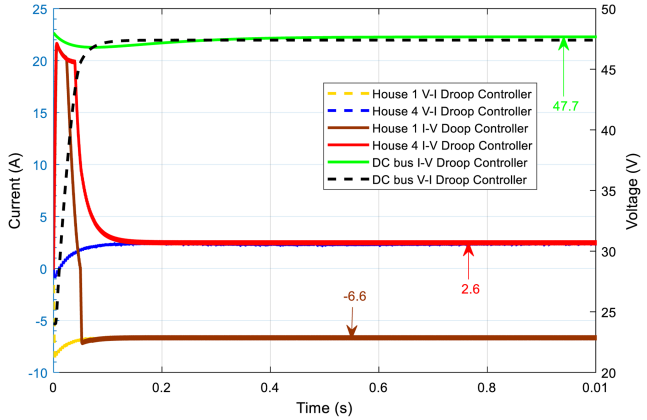

Fig. 9 *Comparative results of current sharing and DC bus voltage for dual-loop V–I droop controller with I–V droop controller for case 1*

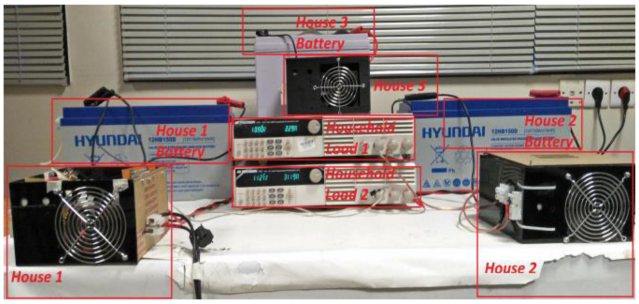

Fig. 10 *Laboratory scale hardware implementation setup*

Table 2 Parameters of hardware implementation

Description of the parameter	Value
number of nanogrids/households	3
input capacitance of each *Conv* b_i	1000 μF
inductance of each *Conv* b_i	700 μH
inductance of each *Conv* a_i	650 μH
DC bus capacitance	6.6 mF
switching frequency for converters	20 kHz
battery capacity for each household	1440 Wh
rated battery charging current	15 A
rated voltage of each battery	12 V
maximum threshold of battery SOC	80%
minimum threshold of battery SOC	30%
reference voltage for DC bus	48 V
converters droop coefficient	0.1 Ω
micro-controller specifications	DSPIC 30F4011
grid battery specification	500 Wh

scenarios of power sharing are evaluated using the proposed control algorithm and are discussed below.

4.2.1 One house is in CCCM and remaining houses are in V–I droop mode: In this scenario, the battery of house 1 is considered below the minimum threshold of SOC, i.e. $SOC_1 = 10\%$; therefore, it is in CCCM. While the batteries of house 2 and house 3 are between the maximum and minimum thresholds of SOC, therefore, these two houses and their associated interface converters are operating in *V–I* droop mode. Two sub-cases are considered for the evaluation of coordinated power sharing such that in case (a) $SOC_2 = 60\% > SOC_3 = 70\%$ and in case (b) $SOC_2 = SOC_1 = 70\%$. In this scenario, both houses will contribute current for the battery charging of house 1 based on their resource availability. The resultant current-sharing characteristics along with grid voltage profile for both cases are shown in Figs. 11 and 12. From Figs. 11 and 12, it can be seen that in case (a), house 3 has relatively higher SOC; therefore, it is contributing a relatively

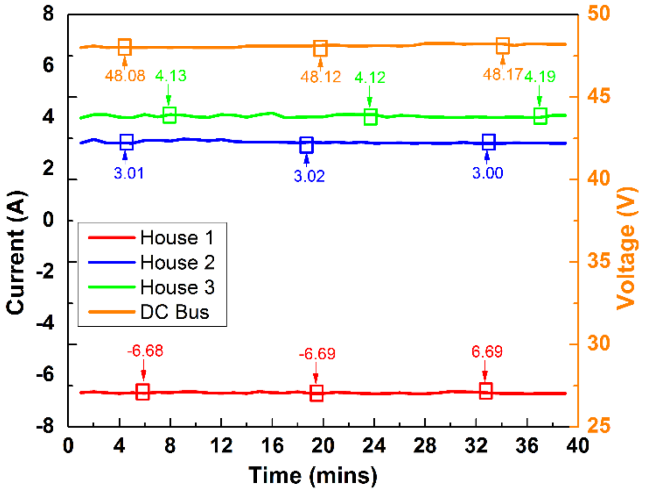

Fig. 11 *Hardware results for current sharing and DC bus voltage in scenario 1, case (a)*

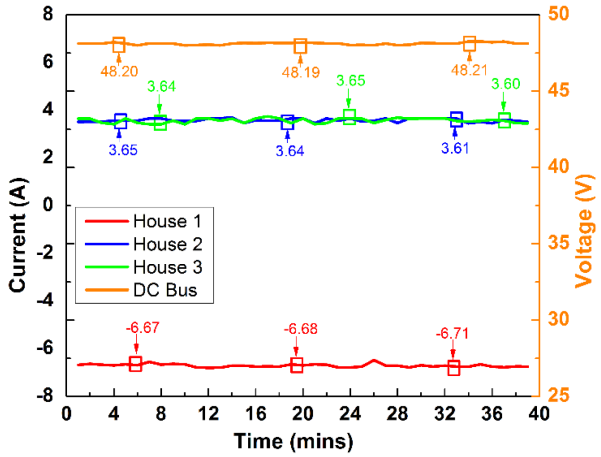

Fig. 12 *Hardware results for current sharing and DC bus voltage in scenario 1, case (b)*

higher amount of current in comparison with house 2, whereas in case (b), both houses are contributing almost equal currents for grid battery charging, because they are operating at equal SOC. Therefore, a coordinated resource sharing is achieved based on the multi-mode adaptive algorithm and resource availability index SOC as demonstrated by the hardware results.

4.2.2 One house is in CCDM and remaining houses are in V–I droop mode: In this scenario, the battery of house 1 is considered above the maximum threshold of SOC, i.e. $SOC_1 = 90\%$; therefore, it is in CCDM. While the batteries of house 2 and house 3 are between the maximum and minimum thresholds of SOC; therefore, these two houses and their associated interface converters are operating in *V–I* droop mode. Two sub-cases are considered for the evaluation of coordinated power sharing such that in case (a) $SOC_2 = 70\% > SOC_3 = 60\%$ and in case (b) $SOC_2 = SOC_3 = 70\%$. In this scenario, both houses will absorb current from the grid battery charging based on their resource availability.

The resultant current-sharing characteristics along with grid voltage profile for both cases are shown in Figs. 13 and 14. From Figs. 13 and 14, it can be seen that in case (a), house 2 has a relatively higher SOC; therefore, it is absorbing the relatively lower amount of current in comparison with house 1, which has relatively higher SOC. While in case (b), both houses are absorbing almost equal current from the house 1 which is operating in CCDM and supplying according to its resource availability, i.e. SOC. Therefore, a coordinated resource sharing is achieved as demonstrated through the hardware results shown in Figs. 13 and 14.

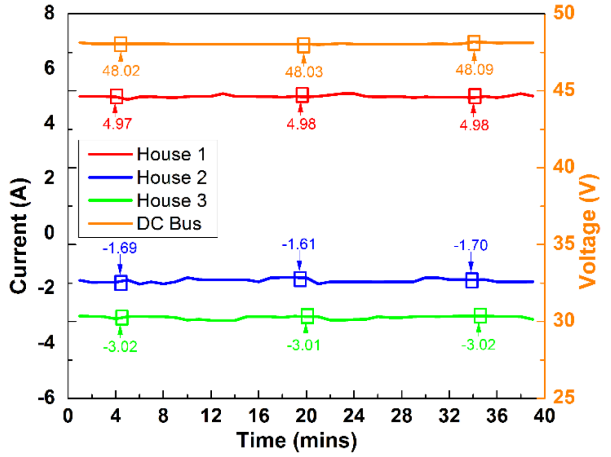

Fig. 13 *Hardware results for current sharing and DC bus voltage in scenario 2, case (a)*

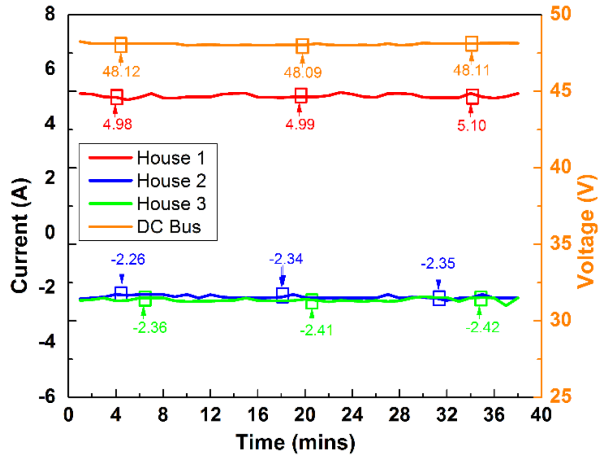

Fig. 14 *Hardware results for current sharing and DC bus voltage in scenario 2, case (b)*

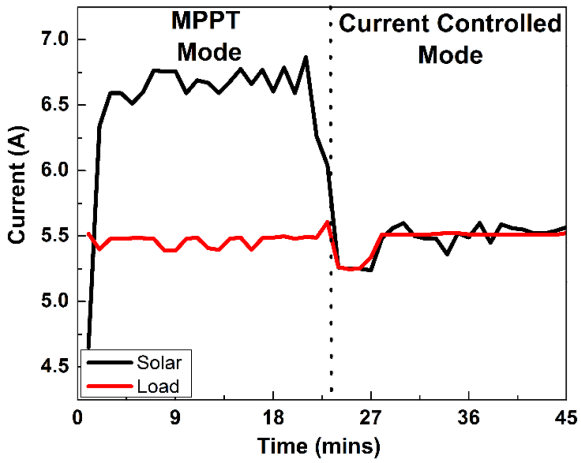

Fig. 15 *Hardware results for the transition between MPPT and CCM in excessive generation condition*

4.2.3 All three houses are in I–V droop mode and excessive generation is available: In this scenario, batteries of all the three houses are above maximum threshold, i.e. $SOC_1 = SOC_2 = SOC_3 =$ 90% and excessive PV generation is available. In this scenario, all three houses will start supplying power to the grid until the grid voltage attains its maximum allowable limit. The current supplied by *Conv* a_1 is shown in Fig. 15. From Fig. 15, it can be seen that at $t = 23$ min, the solar converter changes its mode of operation from MPPT mode to current control mode and it curtails PV generation according to household current requirements, i.e. around 5.5 A.

5 Conclusion

In this work, an adaptive control scheme using dual-loop *V–I* droop is presented and extended control modes for dealing with excessive PV generation conditions are also discussed. The validity of the proposed decentralised control scheme is demonstrated through simulated and measured results. *V–I* droop ensures higher stability margins, while SOC-based variations in droop enable coordinated resource sharing without dedication communication resources. Therefore, distributed architecture with the proposed adaptive control scheme results in (a) lower distribution losses due to unwanted SOC balancing in a distributed architecture, (b) scalability and modularity in terms of future expansions, (c) communication-less coordinated control without dedicated communication infrastructure, and (d) stability over a wide range of operation, even at extreme PV generation and low load utilisation conditions. Therefore, the decentralised control scheme applied to the decentralised architecture of DC microgrid is deemed highly suitable for future rural electrification deployments. Although the decentralised control without dedicated communication infrastructure offers a reduction in the upfront cost of deployment (highly suitable for developing villages with economic limitations), however, for extended applications such as transactive energy, peer-to-peer energy trading, and economic load dispatch, distributed control schemes employing cost-effective and dedicated communication schemes, e.g. power line communication or wireless fidelity-based neighbourhood-level communication techniques are required. These cost-effective communication schemes for transactive energy applications has the tendency to enhance the utility of the distributed DC microgrid architectures and can be regarded as a candidate subject for future research in this area.

6 References

[1] Bergasse, E., Paczynski, W., Dabrowski, M., *et al.*: 'The relationship between energy and socio-economic development in the southern and eastern mediterranean', 2013

[2] Peters, J., Sievert, M.: 'Impacts of rural electrification revisited – the African context', *J. Dev. Effectiveness*, 2016, **8**, pp. 327–345

[3] World Energy Outlook (WEO, 2017): Electricity access database. Available at https://www.iea.org/publications/freepublications/publication/WEO2017SpecialReport_EnergyAccessOutlook.pdf

[4] González-Eguino, M.: 'Energy poverty: an overview', *Renew. Sustain. Energy Rev.*, 2015, **47**, pp. 377–385

[5] Lam, N.L., Smith, K.R., Gauthier, A., *et al.*: 'Kerosene: a review of household uses and their hazards in low- and middle-income countries', *J. Toxicol. Environ. Health B*, 2012, **15**, pp. 396–432

[6] Schnitzer, D., Lounsbury, D.S., Carvallo, J.P., *et al.*: 'Microgrids for rural electrification: a critical review of best practices based on seven case studies', *U.N. Found*, 2014, available at https://rael.Berkeley.edu/publication/microgrids-for-rural-electrification-a-critical-review-of-best-practices-based-on-seven-case-studies, p. 120

[7] Justo, J.J., Mwasilu, F., Lee, J., *et al.*: 'AC-microgrids versus DC-microgrids with distributed energy resources: a review', *Renew. Sustain. Energy Rev.*, 2013, **24**, pp. 387–405

[8] He, G., Victor, D.G.: 'Experiences and lessons from China's success in providing electricity for all', *Resour. Conserv. Recycle*, 2012, **122**, pp. 335–338

[9] Nasir, M., Khan, H.A., Zaffar, N.A., *et al.*: 'Scalable solar dc microgrids: on the path to revolutionizing the electrification architecture of developing communities', *IEEE Electrification Mag.*, 2018, **6**, pp. 63–72

[10] Nasir, M., Zaffar, N.A., Khan, H.A.: 'Analysis on central and distributed architectures of solar powered DC microgrids'. Power Systems Conf. (PSC), Clemson, USA, 2016, pp. 1–6

[11] Hamza, M., Shehroz, M., Fazal, S., *et al.*: 'Design and analysis of solar PV based low-power low-voltage DC microgrid architectures for rural electrification'. Power & Energy Society General Meeting 2017 IEEE, Chicago, USA, 2017, pp. 1–5

[12] Khan, H.A., Ahmad, H.F., Nasir, M., *et al.*: 'Decentralised electric power delivery for rural electrification in Pakistan', *Energy Policy*, 2018, **120**, pp. 312–323

[13] Mishra, S., Ray, O.: 'Advances in nanogrid technology and its integration into rural electrification in India'. 2014 Int. Power Electronics Conf. (IPEC-Hiroshima 2014-ECCE-ASIA), Hiroshima, Japan, 2014, pp. 2707–2713

[14] Palit, D., Sarangi, G.K., Krithika, P.: 'Energising rural India using distributed generation: the case of solar mini-grids in Chhattisgarh state', in (Eds.): '*Mini-grids for rural electrification of developing countries*', (Springer, India, 2014), pp. 313–342

[15] Urpelainen, J.: 'Energy poverty and perceptions of solar power in marginalized communities: survey evidence from Uttar Pradesh', *Renew. Energy*, 2016, **85**, pp. 534–539

[16] Inam, W., Strawser, D., Afridi, K.K., *et al.*: 'Architecture and system analysis of microgrids with peer-to-peer electricity sharing to create a marketplace which enables energy access'. 2015 Ninth Int. Conf. Power Electronics and ECCE Asia (ICPE-ECCE Asia), Seoul, South Korea, 2015, pp. 464–469

[17] Nasir, M., Khan, H.A., Hussain, A., *et al.*: 'Solar PV-based scalable DC microgrid for rural electrification in developing regions', *IEEE Trans. Sustain. Energy*, 2018, **9**, pp. 390–399

[18] Madduri, P.A., Poon, J., Rosa, J., *et al.*: 'Scalable DC microgrids for rural electrification in emerging regions', *IEEE J. Emerg. Sel. Top. Power Electron.*, 2016, **4**, pp. 1195–1205

[19] Groh, S., Philipp, D., Lasch, B.E., *et al.*: 'Swarm electrification-suggesting a paradigm change through building microgrids bottom-up'. 2014 Third Int. Conf. Developments in Renewable Energy Technology (ICDRET), Dhaka, Bangladesh, 2014, pp. 1–2

[20] Dragičević, T., Lu, X., Vasquez, J.C., *et al.*: 'DC microgrids – part I: a review of control strategies and stabilization techniques', *IEEE Trans. Power Electron.*, 2015, **31**, pp. 4876–4891

[21] Amini, M.H., Boroojeni, K.G., Dragičević, T., *et al.*: 'A comprehensive cloud-based real-time simulation framework for oblivious power routing in clusters of DC microgrids'. 2017 IEEE Second Int. Conf. DC Microgrids (ICDCM), Nuremberg, Germany, 2017, pp. 270–273

[22] Moayedi, S., Davoudi, A.: 'Distributed tertiary control of DC microgrid clusters', *IEEE Trans. Power Electron.*, 2015, **31**, pp. 1717–1733

[23] Kou, P., Liang, D., Gao, L.: 'Distributed EMPC of multiple microgrids for coordinated stochastic energy management', *Appl. Energy*, 2017, **185**, pp. 939–952

[24] Li, C., Coelho, E.A.A., Dragičević, T., *et al.*: 'Multiagent-based distributed state of charge balancing control for distributed energy storage units in AC microgrids', *IEEE Trans. Ind. Appl.*, 2016, **53**, pp. 2369–2381

[25] Lu, X., Sun, K., Guerrero, J.M., *et al.*: 'State-of-charge balance using adaptive droop control for distributed energy storage systems in DC microgrid applications', *IEEE Trans. Ind. Electron.*, 2014, **61**, pp. 2804–2815

[26] Nasir, M., Jin, Z., Khan, H.A., *et al.*: 'A decentralized control architecture applied to dc nanogrid clusters for rural electrification in developing regions', *IEEE Trans. Power Electron.*, 2019, **34**, pp. 1773–1785

[27] Gao, F., Bozhko, S., Costabeber, A., *et al.*: 'Comparative stability analysis of droop control approaches in voltage-source-converter-based DC microgrids', *IEEE Trans. Power Electron.*, 2017, **32**, pp. 2395–2415

[28] Jin, Z., Meng, L., Guerrero, J.M.: 'Comparative admittance-based analysis for different droop control approaches in DC microgrids'. 2017 IEEE Second Int. Conf. DC Microgrids (ICDCM), Nuremberg, Germany, 2017, pp. 515–522

[29] Nasir, M., Khan, H.A., Niazi, K.A.K., *et al.*: 'Dual-loop control strategy applied to PV/battery based islanded DC microgrids for swarm electrification of developing regions', *J. Eng.*, 2019, doi: 10.1049/joe.2018.9274

[30] Subudhi, B., Pradhan, R.: 'A comparative study on maximum power point tracking techniques for photovoltaic power systems', *IEEE Trans. Sustain. Energy*, 2013, **4**, pp. 89–98

[31] Nasir, M., Zia, M.F.: 'Global maximum power point tracking algorithm for photovoltaic systems under partial shading conditions'. 2014 16th Int. Power Electronics and Motion Control Conf. and Exposition (PEMC), Antalya, Turkey, 2014, pp. 667–672

[32] Nasir, M., Iqbal, S., Khan, H.A.: 'Optimal planning and design of low-voltage low-power solar DC microgrids', *IEEE Trans. Power Syst.*, 2018, **33**, pp. 2919–2928

[33] Nasir, M., Anees, M., Khan, H.A., *et al.*: 'Integration and decentralized control of standalone solar home systems for off-grid community applications', *IEEE Trans. Ind. Appl.*, 2019, 10.1109/TIA.2019.2911605